Dense-water bottom currents in the Southern Adriatic Sea in spring 2012

Dense-water bottom currents in the Southern Adriatic Sea in spring 2012

Article *in* Marine Geology · September 2015

DOI: 10.1016/j.margeo.2015.09.005

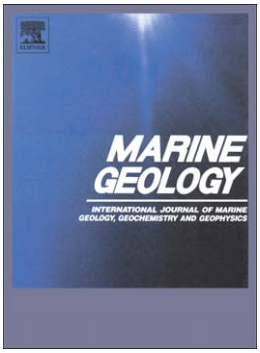

Dense-water bottom currents in the Southern Adriatic Sea in spring 2012

Jacopo Chiggiato, Andrea Bergamasco, Mireno Borghini, Francesco M. Falcieri, Pierpaolo Falco, Leonardo Langone, Stefano Miserocchi, Aniello Russo, Katrin Schroeder

PII: S0025-3227(15)30031-1
DOI: doi: 10.1016/j.margeo.2015.09.005
Reference: MARGO 5344

To appear in: *Marine Geology*

Received date: 1 December 2014
Revised date: 27 August 2015
Accepted date: 6 September 2015

Please cite this article as: Chiggiato, Jacopo, Bergamasco, Andrea, Borghini, Mireno, Falcieri, Francesco M., Falco, Pierpaolo, Langone, Leonardo, Miserocchi, Stefano, Russo, Aniello, Schroeder, Katrin, Dense-water bottom currents in the Southern Adriatic Sea in spring 2012, *Marine Geology* (2015), doi: 10.1016/j.margeo.2015.09.005

Dense-water bottom currents in the Southern Adriatic Sea in spring 2012

Jacopo Chiggiato[1,+], Andrea Bergamasco[1], Mireno Borghini[1], Francesco M. Falcieri[1], Pierpaolo Falco[2], Leonardo Langone[1], Stefano Miserocchi[1], Aniello Russo[1,3,*], Katrin Schroeder[1]

1 Istituto di Scienze Marine, Consiglio Nazionale delle Ricerche, CNR-ISMAR, Italy

2 Dipartimento di Scienze e Tecnologie, DIST – UniParthenope, Italy

3 DISVA, Universita' Politecnica delle Marche, Italy

* now at CMRE, NATO Science and Technology Organization, Italy

+ corresponding author: email jacopo.chiggiato@ismar.cnr.it, tel. (+39) 041.2407.945, fax (+39) 041.2407.940

Abstract

In February 2012, a severe cold spell in the European region triggered a massive production of very dense water on the northern Mediterranean Sea shelves. The spreading phase of the newly formed dense water was extensively studied in the Adriatic Sea by means of 2 ship surveys and 5 moorings fully equipped to monitor the flow of the bottom layer. For the Adriatic Sea, opposite to the Gulf of Lions, the area of cascading is far from the source area and this implies substantial modifications, adjustments and dilution of the source water mass along its path, with a spreading phase lasting several months. Indeed all the moorings detected events, although weaker than in the preceding months, until June 2012. The surveys detected 2 branches of NAdDW on the shelf, the first branch not denser than 29.7 kg/m^3 and the second branch not denser than 29.5 kg/m^3. Despite the extremely dense water generated in the Northern Adriatic, during events of dense-water flow, moorings recorded temperatures generally between 12.5 and 13 °C, seldom less. Temperatures along the shelf break also did not fall below 13 °C at depths greater than 400m. Turbulent mixing, therefore, heavily modified the cascading plumes, which left the shelf with thicknesses between 10 and 30m. Mooring data in the lowermost 100 mab suggest that the thickness of the cascading layer increased by several tens of meters downslope, as a consequence of entrainment. Detraining frictional layers as well as locations of active

cascading were identified mostly by isolated casts, highlighting the submesoscale domain of the downsloping plumes. The use of LADCP data allowed identify very energetic bottom flow (40 - 50 cm/s in many locations), with otherwise little signature in tracers, not previously observed. The Bari Canyon System (BCS) was so far recognized as a hot spot for cascading in the Southern Adriatic. However, during the 2012 event, this is not the only preferred site for cascading. Significant dense flow was detected in other locations. The northernmost mooring site, closer to the inception of the cascading process, in particular showed active cascading and several dynamical differences from the BCS: denser water with thinner boundary layer, events organized in multiple pulses with sub-inertial periodicity and with very short duration (12 hours to 1 day) that is generally not seen in other locations.

1 Introduction

The shallow and broad continental shelf of the Northern Adriatic is one of the shelves of the northern Mediterranean Sea known to be prone to dense shelf water production (Hendershott and Rizzoli, 1976; Artegiani and Salusti, 1987; Artegiani et al 1989, Vilibić and Supić, 2005). Intense winter cooling and evaporation, associated with dry and cold north-easterlies (Bora winds), favours the production of a water mass known as Northern Adriatic Dense Water (NAdDW). The process of generation is principally temperature driven (Shapiro et al., 2003), although lateral advection of salinity from the Southern Adriatic, as well as the freshwater discharge from rivers along the coast, do have an impact in the preconditioning phase in assisting or limiting the production.

The newly generated dense water moves southward along the isobaths of the Italian continental shelf and slope as a buoyancy driven current. If dense enough, a portion of the water mass fills the Jabuka Pit, a 270m deep depression where NadDW accumulates, eventually flushing lighter and older water masses (Bergamasco et al 1999; Vilibić and Supić, 2005; Marini et al., this issue). Usually after 2-4 months (Vilibić and Orlić 2002), the

buoyancy current travelling along the Italian shelf reaches the Southern Adriatic, where it sinks through successive cascading events. A known site for cascading events is the Bari Canyon System (BCS), as anticipated by pioneer works in the '80s (e.g., Bignami et al. 1990a, 1990b) and recently observed during a dedicated field study (e.g., Turchetto et al., 2007). While descending the slope, the plume entrains Levantine Intermediate Water (LIW), becoming warmer and saltier. The cascading process plays a relevant role in biogeochemical cycles (Shapiro et al., 2003), as cascading NAdDW ventilates the intermediate and abyssal layers of the Southern Adriatic and sustains transport of particles and organic matter (Turchetto et al., 2007; Tesi et al., 2008; Cantoni et al.; Langone et al.; Taviani et al. this issue). Despite the biogeochemical relevance, due to inherent difficulties in observing cascading events, there are still open issues not fully addressed by sporadic ship-borne surveys. While waiting for a distributed network of moving platforms to allow for high-resolution monitoring of the flow of dense water (e.g., Vilibić and Mihanović, 2013), recently the scientific community concentrated efforts on moorings to monitor the flow of dense water in various key areas of the Southern Adriatic (e.g., Bensi et al. 2013; Turchetto et al., 2007; Langone et al., this issue).

In February 2012, the European region experienced a 2-week severe cold spell, sustained by a large Siberian high and associated blocking of the Atlantic flow. This synoptic configuration allowed for retrogression of westward flow of dry and cold artic air masses from eastern Russia along the southern flank of the anticyclone all the way to Europe, causing temperature as low as -40 °C in northeastern Europe and –10° to –20°C in central Europe, with significant snowfall in southern Europe associated with deep lows in the Mediterranean Sea (Grazzini, 2013). The Northern Adriatic was heavily impacted by this cold spell, which caused large decrease of surface temperature and the onset of severe northeasterly Bora winds (see figure 2(b) in Raicich et al., 2013), blowing almost continuously and intermittently reinforced by cyclogenesis in the western Mediterranean. A significant heat loss took place in the basin, inducing water temperature as low as 4 °C and potential density anomaly of 30.6 kg/m^3 (Mihanovic et al., 2013). Raicich et al. (2013) computed the ratio between temperature-induced and salinity-induced buoyancy loss by air-sea interaction during the event in the

Gulf of Trieste (North-eastern Adriatic), with the former roughly three times larger than the latter, supporting the general idea of temperature-controlled dense-water production in the Northern Adriatic. Yet, the not-negligible evaporation during the event (Raicich et al., 2013) and dry atmospheric conditions with consequent lower-than-usual river discharge in the preceding months (Mihanović et al., 2013; Janeković et al., 2014) did contribute to exceptional seawater density. Also other shelves of the Mediterranean Sea experienced a massive production of dense water in February 2012 (e.g., Gulf of Lions; Durrieu de Madron, 2013), although with potential density anomaly values (29.7 kg/m^3) not as large as in the Northern Adriatic Sea.

Following this severe winter 2012 cold outbreak in the northern Adriatic, CNR-ISMAR set up two rapid-response cruises to study the occurrence, amount, timing and properties of the newly formed dense water, aiming at characterizing the vertical structure and spatiotemporal variability of the benthic layer and its modification during down-flowing regimes. The Southern Adriatic was therefore extensively sampled by the R/V Minerva Uno (leg 1, 23 March – 2 April 2012) and R/V Urania (leg 2, 14-20 April 2012) with CTD-rosettes equipped with additional sensors for fluorescence, dissolved oxygen, Lowered Acoustic Doppler Current Profilers (LADCP) as well as ship-borne ADCP and XBTs. In addition to the 3D snapshot carried out during the surveys, five moorings continuously measured temperature, salinity, currents and downward particle fluxes by means of SBEs, ADCPs and automatic sediment traps. Mooring locations were carefully chosen based on depositional and erosional features suggestive of intense bottom flow (Foglini et al., this issue) and key areas identified by means of numerical ocean-model experiments.

2 Data

Two cruises were carried out to monitor dense-water flow in the Southern Adriatic (figure 1), in late March and mid April, respectively, by the Italian R/V Minerva-Uno and the Italian R/V Urania. At all the hydrological stations, pressure (P), salinity (S), potential temperature (θ) and dissolved oxygen concentration (DO) were

obtained with a CTD-rosette system consisting of a CTD SBE 911 plus and a General Oceanics rosette with 12 12-l Niskin Bottles. The probe has been calibrated before the cruises in the CMRE (formerly NURC) calibration bath in La Spezia (Italy). Temperature measurements were performed with two SBE-3/F thermometer, which had an accuracy of order (10^{-3}) °C. Conductivity measurements were performed with two SBE-4 sensors, which had an accuracy of order (10^{-4}) S/m. DO was measured with a SBE-43 sensor (resolution 4.3 µM), and data were checked against Winkler titration. The rosette also hosted two RDI WorkHorse 300-kHz lowered Acoustic Doppler Current Profilers (LADCP) to retrieve velocity measurements during the cast. Postprocessed LADCP data have 6 cm/s accuracy. LADCP data are not detided. Estimates of tidal currents corresponding to the LADCP stations carried out by means of a finite element model on the Adriatic Sea (Bellafiore et al., 2008) did not show significant tidal currents (few cm/s, D. Bellafiore, personal communication). In addition, several Sippican expendable Bathythermographs (XBT) were launched for rapid observation of dense-water flow and in order to increase the horizontal resolution of temperature measurements of dense-water plumes (see figure 2).

Five moorings have been deployed in order to monitor the flow of dense water, equipped with current-meters, conductivity-temperature-depth (CTD) sensors and Acoustic Doppler Current Profilers (ADCP). Four of them (namely BB, CC, DD and FF, see figure 2) were specifically devoted to detect cascading events down the shelf. For this reason, instruments are placed in the first 100m from the bottom with a similar sampling strategy: Aandeera RCM current-meter at roughly 8m above bottom (hereinafter mab), SBE temperature/conductivity sensor at 12 mab, SBE temperature sensor at 18 mab (in all but CC mooring) and downward looking RDI 300 KHz ADCP at 100 mab (in all but DD mooring, equipped instead with a couple of current meters). Mooring EE was meant to monitor also open-ocean convection events; thus, its design is different, with several temperature sensors and current meters in a 1000-m-long line (unfortunately, several sensors failed). Two locations out of five were monitored in the past (BB and CC, in the BCS; see Rubino et al. 2012; Turchetto et al., 2007). As said, moorings locations were based on depositional and erosional features suggestive of intense bottom flow as well as numerical ocean-model experiments.

3 Water Masses and Stratification

The theta-S plot (figure 3) allows to identify the water masses intercepted by the CTD surveys. The first cruise (leg 1) has been divided in two parts (a,b) due to severe weather. The NAdDW observed was abundant in Leg 1a and barely present in leg 1b, as it is also evident from the bottom water properties displayed in figures 4 (leg 1a) and 5 (leg 1b). This is in agreement with the intermittent, pulsing dynamics of the NAdDW flow in the area, as anticipated by Bignami et al., 1990b following Killworth (1977). During Leg1a, the NAdDW signal was clearly identified, with a potential density anomaly of 29.7 kg/m^3 and θ <11 °C. The salinity was greater than the usual value in the region due to the reduced river runoff during the preconditioning phase in the Northern Adriatic Sea (Janeković et al. 2014). This salinity hampers the identification of NAdDW from MAdDW based on T and S only, and additional parameters are necessary. Based on NO_3+NO_2 concentrations, Cantoni et al. (this issue), identified this water mass as NAdDW. During Leg 1b, the NAdDW was definitely less with an observed potential density anomaly barely exceeding 29.3 kg/m^3. During Leg 2 (figure 3), a branch of NAdDW was again clearly identifiable, with potential density anomaly exceeding 29.5 kg/m^3, although less dense compared to Leg 1a. In addition, the content in salinity is higher and the NAdDW branch seems to point to a different end point with respect to Leg 1a. This water mass was either generated in an area of higher salinity (e.g., northeastern Adriatic), or mixed more with saltier waters in the middle Adriatic. During leg 2, most of the signal of dense water was confined to the north (figure 6).

The different abundance of dense water detected during the sampling periods also reflects on the vertical stratification (figure 7). Off the shelf break (< 180m in figure 7), values were barely below 13 °C during Leg 1. This observation reinforces the evidence of the low content of NAdDW in the survey during Leg 1b, because during Leg 1a most of the stations were on the shelf. In Leg 2, values as low as 12 °C were instead found down to 400m (figure 7), as a consequence of cascading plumes. Evidence of LIW was not always detectable, as the survey occurred immediately after winter mixing and intermediate open-ocean convection to a depth of 600m

(not shown; see also Bensi et al., 2013). Thus, the water mass was vertically homogeneous. Instead, the subsurface water, away from the shelf, was significantly rich in salinity. This higher salinity layer was concentrated in the upper 200 m (figure 7). As a consequence of open-ocean convection, this layer was missing in several stations offshore (not shown). Intrusion of high-salinity water masses are usually considered modified LIW; however the very shallow depth and high content of dissolved oxygen (~5.7 ml/l), suggestive of ventilation, is not consistent with a classical LIW definition. This water mass was more likely Ionian Surface Water (ISW). Intrusion of LIW, marked by local maxima of salinity and minima of DO (figure 7), were instead detected between 200-600m. During leg 1b, with many CTD stations off the shelf break, the presence of Adriatic Deep Water (ADW) can be noted. It is worth noticing the variable oxygen content in the deep layer (600-1200): in some stations DO is low (4.7 ml/l) and, in other cases, is relatively high (5.2 ml/l); the latter indicating that new ADW was formed.

4 Characteristics of dense-water plumes on the shelf

In the northern part of the domain, two CTD transects define the plume of dense water intercepted travelling across the shelf. Both transects are from leg 1a, during the intense flow of dense water. The southern transect B (see location on figure 4) was carried out on 24 March , while the northernmost transect A (figure 4) one day later, 25 March. The signal of dense water in the latter transect was weaker; cross-checking with the time series in FF mooring (figure 14, discussed later), the transect A seems to sample a tail of an impulse. The dense-water plume on transect A (figure 8) was 20-30m thick and 50 km wide. Two local maxima on the shelf were detected at 100m, 130m. These levels have been noticed several times in past field campaigns. The first Rossby internal radius of deformation in the two densest stations (043 and 039b, figure 9) was about 3 km (see table 1). This estimate has been done using 1 ½ reduce gravity model, disregarding the surface layer undergoing re-stratification. Given this internal radius, the sampling strategy of CTD casts every some 3 nm and XBT between

can be considered the minimum resolution to resolve the horizontal structures of the cores. The plume as a whole was larger than the internal radius, and the thickness was larger than the frictional layer; the plume could therefore be expected to be in geostrophic balance to the lowest order (Wåhlin and Walin, 2001). At 180m, there was another local maximum, likely denoting a descending flow as indicated by instantaneous LADCP data in 039b (northernmost arrow in figure 5a), which suggest cross-isobath bottom flow. In addition, the presence of a seafloor ridge (figure 5a) could trigger an increase of transport downslope (Muench et al., 2009, Darelius and Wåhlin, 2007), consistent with the development of a furrows field downstream.

The water found in the southern transect (figure 8) was the densest of the entire survey. The shape of the plume resembled a typical asymmetrical behavior (e.g., in Wåhlin and Walin, 2001). The upper edge adjusted to a roughly horizontal interface. According to Wåhlin and Walin (2001), this is a lower state of potential energy, with the lower edge frictionally controlled moving downslope with a reduced thickness, detraining from the plume. From this transect, two stations are discussed: 029 and 030 (figure 10, see also table 1). Although separated by 3 nm only, these two stations are proxies of two different regimes. In both cases, the surface layer, undergoing re-stratification by lateral advection, was 20m thick. However, in CTD 029, the salinity was less, due to the impact, on the shelf, of riverine waters. Furthermore, in CTD 029 an intermediate boundary layer and a well-mixed bottom layer were detected. In CTD 030, between 20m and 100m, there was an intrusion of greater salinity, greater temperature ISW, which was not visible in CTD 029, indicating that this station was affected instead by open-ocean water masses. In CTD 030, the well mixed bottom layer was missing and the boundary layer was composed by a vertical sequence of dense water with peaks at 130m, 150m, 180m. The thickness of the plume in this location was indeed comparable to δ, as predicted by Wåhlin and Walin (2001) model. In addition, the bottom flow was faster (40 cm/s), based on LADCP instantaneous data. These data also indicate intense baroclinic velocity in the whole layer with cross-isobaths direction, suggestive of cascading initiated.

5 Cascading along the southern Adriatic shelf break

Canyons are known hot spots for cascading and in general, for cross-margin exchange (Wåhlin, 2002; Canals et al. 2006; Allen and Durrieu de Madron, 2009). The BCS has been recently studied by Turchetto et al. (2007), finding that the total mass flux in the canyons was greater than on adjacent slopes. However, they also found a not negligible downward transport also on open slopes. Rubino et al. (2012), based on model simulations, identified other regions favorable to cascading in addition to the BCS: the Gondola Slide (figure 1, just south the FF area) and the slope downstream the BCS (roughly the DD area). Both sites (FF and DD area) experience an increased steepness of the continental slope, with advective terms more likely to break geostrophic constraints (i.e., larger Rossby number regimes, Allen and Durrieu de Madron, 2009, Matsumura and Hasumi, 2011) and thus, downslope motion is arguably increased.

All moorings (figure 2, right panel) were affected by the passage of dense gravity currents, indicated by concurrent signal of low temperature (or high density) and intense currents. Figure 11 shows time series of potential temperature and currents speed from the moored instruments at respectively 12 and 8 mab. Currents were often up to 50 cm/s, even at locations in the deep pit of the Southern Adriatic (mooring EE). During intense current events, temperature dropped. Largest velocities were found in BB, but yet comparable also in FF and in EE. Currents in CC were generally lower than in BB, in agreement with the time series discussed by Turchetto et al. (2007). Being lower the alongshore distance from the source, mooring FF consequently showed the lower temperature. Arguably, the farther the current goes, the more diluted is the NAdDW, as it was at DD. This has indeed implications on the potential energy released during cascading. Model results by Rubino et al. (2012) are suggestive that larger density contrast and thickness of the plume offshore the Gargano Peninsula provides larger velocities, at least in the canyons.

Time-series presented in figure 11 suggest that events are intermittent, with periodicities that differ from site to site. The mooring FF showed a remarkable variability in the occurrence of events of dense (cold) water flow,

organized in trains or packets of short-lived pulses. A wavelet analysis was performed to give quantitative estimate of this behavior. The analysis was carried out on potential density time-series, rather than on currents, using a Morlet mother wavelet and the MatLab® toolbox provided by Grinsted et al. (2004). The potential density was selected to identify mutual behavior focusing only on dense water flow episodes (i.e., temporary increase in potential density) while currents on the bottom experiences also fluctuations associated to different dynamics (e.g., geostrophic flow), not necessarily connected to downslope activity. The analysis indicates that the short-lived pulses had sub-inertial period of 1.6 days, which can be ascribed to baroclinic instabilities of the overflow (e.g., Smith 1976). Other moorings showed longer periods (3 to 4 days on currents, longer based on density), underlying the peculiar behavior of the FF site.

During cascading events, current directions were well organized (figure 12). In FF, the direction was approximately $\pi/2$ to the left with respect to the isobaths down-current, indicating ageostrophic dynamics. BB showed a bimodal behavior: one direction was along the canyon axis (110°), associated to coldest temperatures, and one was southward, which is not directly associated to cascading, being along the direction of the isobaths upstream. Yet, the southward component is nonetheless associated to relatively cold water mass, therefore can be indirectly associated to cascading, i.e., laying downstream of a geostrophycally adjusted downslope flow. Turchetto et al. (2007) documented the same bimodal behavior in an earlier interval of several years; thus, it seems a robust feature of the flow at that location. Instead, CC was not bimodal as BB. At this location the preferred direction was clearly the along-canyon one, while the southward flow was scarcely present. As anticipated by Trincardi et al. (2007), this is a consequence of the topographic feature downstream next to the canyon, forcing the flow to deflect. Based on CTD and LADCP data collected, the topographic Froude number was $O(10^{-2})$, implying blocking (Smith, 1979). In this case, the natural length-scale, when the flow starts to deflect because of the ridge, is the internal Rossby radius (Chen and Smith, 1987), and BB might be far enough. Currents in DD had less dominant direction, with a broad range between roughly 80° (across

slope) to 130° (along slope). EE also showed a preferred direction, associated to coldest temperatures, that is the eastward flow controlled again by the local seamount.

Cross-correlations between moorings data have been analyses by means of lagged correlation on potential density time-series at 12 mab. The same analysis was carried out on currents at 8 mab. As done for the wavelet analysis, cross correlations have been computed on potential density time-series. Lagged correlations are generally high (0.5 – 0.6), with the noticeable peak on BB vs. CC (0.86).Assuming that the signal passing on FF later reaches EE, it reaches EE three days later. EE is also arguably affected by the flow coming from Pelagruza. Assuming that the flow on the shelf that is cascading in FF is later cascading also in BB and CC, the signal arrives respectively 3 and 3.27 days later. Note that the delay between BB and CC, 8 hours, is consistent with results from 2004/2005 mooring campaign (Rubino et al. 2012). The signal then reaches DD 4.5 days later.

The area of the mooring FF, north of Gondola Slide was continuously sampled by the mooring and with CTD in both cruises. In particular during the second leg, this area was interested by active spilling. Several CTD stations were carried out upstream mooring FF, most of them being on the shelf or in the upper part of the slope (figure 13). All stations in the area were carried out within twelve hours: the first stations 000 and 068 on 19 April early afternoon, then the research vessel moved north first, to start the zonal transects going back south, however without repeating stations already done. This means that station 009, 066 and 065 were done actually twelve hours later than 068, a period comparable to the duration of a cascading impulse, thus, eventually breaking sinopticity assumptions. In fact, pulses on FF lasted several hours, maybe up to a day, no longer (figure 14).

After careful check of CTD and LADCP profiles, the top of the benthic layer (BL) was marked by waters $\theta < 12.9$ °C. Thickness of the BL was generally 20-30m, with the thickest on station 068. Here the transport at the bottom was clearly cross-isobath, with a sub-layer of roughly 10m directly influenced by friction and pointing toward FF. The station was roughly 15 km far from FF assuming a nearly direct path, which would be, with a

velocity of 0.5 m/s, less than 10 hours. Cross-checking with the time series from the mooring (figure 14), it seems that the flow passing on 068 could be linked with the event passing in FF on 20-21 April. The flow measured later, less energetic (station 066) or significantly warmer (station 069), thus represents a snapshot of the tail of the pulse.

The thickness of the benthic layer (denoted here by a velocity threshold of 20 cm/s from ADCP data) was between 30 and 70m. In particular, the event recorded on 20 April showed an active layer at mooring location of roughly 40m (not shown). On the shelf, based on CTD068 (LADCP included) data, the vein directed toward FF was roughly 20m thick. Down the shelf, the thickness of the bottom layer had doubled, bulk estimate that is also consistent with a θ change from 12°C (CTD068) to 12.8 °C (mooring, 8 mab), considering mixing with ambient θ of 13.8 (as from nearby unperturbed offshore CTD). θ data on the shelf during leg 2 were not colder than 11.5 °C, thus temperature change compared to FF records was 1.3 °C. A similar drop was observed during leg 1, when θ on the shelf of 11 °C was found while mooring data were recording 12.5 °C.

Using the internal Rossby radius R as natural length-scale of the plume (2.6 km at station 068, average velocity of 0.45 m/s and layer thickness 20m), the along-flow transport of dense water was 0.024 Sv. Estimate of transport across the full transect is prevented by lack of sinopticity.

The dynamical picture in the BCS emerging from the hydrographic data is different. Surveys did not sample significant flow of cascading NAdDW at this location, all coming right after not significant events. LADCP values during Leg 2 survey were almost all showing a geostrophic direction (figure 6), likely as a consequence of adjustment after cascading events. However, in few CTDs, the signal of dense water plumes was detectable, as in CTD014 (figure 15) where there was a very thin layer of dense water and from CTD017 (figure 15), where there was a remarkable example of the importance of using LADCP data as complement: the signature on tracers was very weak, while LADCP detected a 100m thick energetic layer oriented down-channel.

The dynamical structure of the benthic layer downstream the two canyons, although adjacent, was dissimilar, as well as it was dissimilar from the structure in FF. Figure 16 shows the average dynamical structure of the lower 100 mab during cascading events only. Here cascading is defined by 8 mab velocities larger than 30 cm/s. Cross-checking with figure 12, using this threshold events are uniquely identified in FF and CC; while for BB an additional constraint has been used (current direction at the bottom between 100 and 130 degrees) to select the down-canyon flow only. FF showed an active layer not thicker, on average, than 40m. At only that depth velocities started to veer from along-slope (in the upper part of FF 100 mab, there was intrusion of LIW, as deducted from CTDs, not shown) to downslope and magnitude increased faster than in the other moorings, depicting a shallower and faster bottom current. BB and CC had same profile below 40 mab; above that depth however, BB was affected by geostrophic flow associated to warmer temperature (not shown). It has been mentioned before that in CC this flow was absent likely due to the deflecting effect of the very close canyon wall, downstream. This wall is also supposed to increase the dense water transport inside the canyon (Wahlin, 2002, Jiang and Garwood, 1998). In fact, above 40 mab, currents in CC were stronger than in BB and uniformly oriented down canyon. Note that bottom average velocities from 8 mab current meters in all cases are remarkably similar, some 40 cm/s.

6. Summary and Conclusions

The cold spell of winter 2012 triggered a massive production of very dense water in the northern Mediterranean Sea shelves (Durrieu de Madron et al., 2013, Mihanović et al 2013). The spreading phase of the newly formed dense water was extensively studied both in the Gulf of Lions by, e.g., Durrieu de Madron et al. (2013) and in the Adriatic Sea (this issue). In the Adriatic Sea, in particular, the dense water bottom flow was monitored by means of 2 R/V surveys and 5 moorings fully equipped in the lower 100 mab. In the Adriatic Sea, opposite to the Gulf of Lions, the area of cascading is far from the source area and this implies substantial modifications, adjustments and dilution of the source water mass along its path, with a spreading phase lasting several months: still in June 2012 events were detected by the moorings, although weaker than in the

preceding months. Due to the modification along its path, the NAdDW observed in the southern Adriatic was considerably lighter than the source mass generated in the Northern Adriatic, where the potential density anomaly was higher than 30 kg/m^3 (Mihanović et al, 2012). The surveys carried out by the R/Vs detected 2 branches of NAdDW travelling on the shelf, the first branch not denser than 29.7 kg/m^3 and the second branch not denser than 29.5 kg/m^3. Despite the extremely dense water generated in the Northern Adriatic, during events of dense water flow, moorings recorded temperature generally between 12.5 and 13 °C, seldom lower. Collected CTD data in locations off the shelf also did not fall below temperature values of 13 °C beneath 400m. Turbulent mixing therefore heavily modified the cascading plumes, although it should be considered that the thickness of the plumes on the shelf was between 10 and 30m, i.e., one order of magnitude lower than in the Gulf of Lions (see Durrieu de Madron et al., 2013). Moorings data in the lowermost 100 mab suggested that the thickness of the cascading layer increased by several tens of meters downslope, as a consequence of entrainment. Plumes travelling on the shelf were wider compared to the Rossby radius (~3 km) and thick compared to frictional boundary layer, therefore expected to be in near geostrophic equilibrium. At least in the area of the most proximal mooring (FF) however, detraining frictional layers as well as locations of active cascading were identified, mostly by isolated casts, highlighting the submesoscale domain of the downsloping plumes. Modeling these processes requires then resolution able to resolve the submesoscale and very high resolution in the bottom layer, in order to simulate the detraining frictional layer that is O(10^0) m, hardly thicker. The design of experiment, including moorings, XBT and LADCP, proved to, at least partially, overcome inherent limitations associated to the small scale of dense water plumes and their intermittent nature. It should be noted that the use of LADCP data allowed identify very energetic bottom flows (40 - 50 cm/s in many locations), with otherwise little signature in tracers, not previously observed.

The BCS was so far recognized as hot spot for cascading in the Southern Adriatic. However, it is not the only preferred site for cascading. Significant dense flow was detected near the FF site and, to a lower extent, to the south of the canyons. Both sites (FF and DD area) experience an increased steepness of the continental slope,

with advective terms more likely to break geostrophic constraints (Allen and Durrieu de Madron, 2009, Matsumura and Hasumi, 2011). The FF site showed several dynamical differences from the BCS: denser water with shallower boundary layer, events organized in multiple impulses with sub-inertial periodicity and with very short duration (12 hours to 1 day) that is not seen in other moorings. Even the canyons in the BCS showed dynamical differences despite the mutual proximity, both in the along-channel flow and in the interaction with the large scale transit of LIW, suppressed in the lowermost 100 mab in CC as a consequence of the topographic ridge downstream. If we consider also mooring AA in Turchetto et al. (2007) and modeling results by Rubino et al. (2012), as well as inferences from numerical simulations that not only canyons but ridges, small scale corrugations, their orientations and geometrical size do play a role (Muench et al., 2009, Darelius and Wåhlin, 2007, Wåhlin, A., 2002 and 2004, Matsumura and Hasumi, 2011), cascades down the Southern Adriatic shelf break should be considered a complex, multi-scale, ubiquitous process with peculiar characteristics location by location, depending on the interplay between the incoming dense water flow and the topographic control. This poses a substantial challenge in observing the process as a whole, meanwhile state-of-the-art numerical modeling exercises (e.g., Rubino et al., 2012, Bonaldo et al., this issue, Carniel et al. this issue) can overcome these difficulties shading lights on the undersampled small scale variability.

Acknowledgements

ODW-2012 campaign was partially supported by the project COCONET (GA # 287844) of the European Commission and the Italian Flagship project RITMARE. JC and KS acknowledge also partial support from the project OCEAN-CERTAIN (GA # 603773) of the European Commission.

References

Allen, S. E. and Durrieu de Madron, X.: A review of the role of submarine canyons in deep-ocean exchange with the shelf, Ocean Sci., 5, 607–650, 2009.

Artegiani, A. and Salusti, E.: Field observation of the flow of dense water on the bottom of the Adriatic Sea during the winter of 1981, Oceanol. Acta, 10, 387–391, 1987.

Artegiani, A., Azzolini, R., Salusti, E., 1989. On the dense water in the Adriatic Sea. Oceanologica Acta, 12, 151-160.

Bellafiore, D., Umgiesser, G., Cucco, A., 2008. Modeling the water exchanges between the Venice Lagoon and the Adriatic Sea. Ocean Dynamics, 58, 397-413.

Bensi, M., V. Cardin, A. Rubino, G. Notarstefano, and P.-M. Poulain (2013), Effects of winter convection on the deep layer of the Southern Adriatic Sea in 2012, J. Geophys. Res., 118, 6064–6075, doi:10.1002/2013JC009432.

Bergamasco, A., Oguz, T., and Malanotte-Rizzoli, P.: Modeling dense water mass formation and winter circulation in the northern and central Adriatic Sea, J. Mar. Syst., 20, 279–300, 1999.

Bignami, F., G. Mattietti, A. Rotundi, and E. Salusti, 1990a: On a Sugimoto–Whitehead effect in the Mediterranean Sea: Fall and mixing of a bottom current in the Bari canyon, Southern Adriatic Sea. Deep-Sea Res., 37, 657–665.

Bignami, F., Salusti, E., Schiarini, S., 1990b. Observations on a bottom vein of dense water in the Southern Adriatic and Ionian Seas. Journal of Geophysical Research,95, 7249-7259.

Bonaldo, D., A. Benetazzo, A. Bergamasco; E. Campiani; F. Foglini; M. Sclavo; F. Trincardi; S. Carniel. Interactions among continental margin morphology, deep Adriatic circulation and bedform patterns, this issue.

Canals, M., P. Puig, X. Durrieu de Madron, S. Heussner, A. Palanques, and J. Fabres (2006), Flushing submarine canyons, Nature, 444, 354–357.

Cantoni, C.,A. Luchetta, J. Chiggiato, S. Cozzi, K. Schroeder, L. Langone , Dense water flow and carbonate system in the southern Adriatic: a focus on the 2012 event. This issue.

Chen, W.D., and R.B. Smith. 1987. Blocking and deflection of airflow by the Alps. Mon. Weather Rev. 115:2578-2597.

Carniel, S., F. Trincardi, D. Bonaldo, A. Benetazzo, A. Bergamasco, A. Boldrin; F. M Falcieri, L. Langone; M. Sclavo, Off-shelf fluxes across the southern Adriatic margin: factors controlling dense-water-driven transport phenomena, this issue.

Darelius, E. and A. Wåhlin, 2007. Downward flow of dense water leaning against a topographic ridge. Deep-Sea Research part I, 54 (7), 1173-1188.

Foglini, F., E. Campiani, F. Trincardi. The reshaping of the South West Adriatic Margin by cascading of dense shelf waters, this issue.

Grazzini, F, 2013. Cold spell prediction beyond a week: extreme snowfall events in February 2012 in Italy ECMWF Newsletter 08/2013; 136(Summer 2013):32-36.

Grinsted, A., Moore, J. C., Jevrejeva, S., 2004. Application of the cross wavelet transform and wavelet coherence to geophysical time series, Nonlinear Processes in Geophysics 11: 561–566.

Hendershott, M. C., and P. Rizzoli, 1976: The winter circulation in the Adriatic Sea. Deep-Sea Res., 23, 353–373.

Ivanov, V. V., G. I. Shapiro, J. M. Huthnance, D. L. Aleynik, and P. N. Golovin (2004), Cascades of dense water around the world ocean, Prog. Oceanogr., 60, 47–98, doi:10.1016/j.pocean.2003.12.002.

Janeković, I., Mihanović, H., Vilibić, I., Tuder, M., 2014. Extreme cooling and dense water formation estimates in open and coastal regions of the Adriatic Sea during the winter of 2012. Journal of Geophysical Research: Oceans, 3200-3218.

Jiang, L., Garwood, R. W., 1996. Three-dimensional Simulations of overflows on continental slopes. Journal of Physical Oceanography, 26, 1214-1233.

Killworth, P., 1977. Mixing on the Weddel Sea continental slope. Deep Sea Research, 24, 427-448.

Langone L., I. Conese, S. Miserocchi, A. Boldrin, D. Bonaldo, S. Carniel, J. Chiggiato, M. Turchetto, M. Borghini, T. Tesi.. Dynamics of particles along the western margin of the Southern Adriatic: processes involved in transferring particulate matter to the deep basin, this issue..

Marini, M., V. Maselli, A. Campanelli, F. Foglini, F. Grilli, Role of the Mid-Adriatic Deep in dense water interception and modification, this issue.

Matsumura, Y., Hasumi, H., 2011. Dynamics of cross-isobath dense water transport induced by slope topography. Journal of Physical Oceanography, 41, 2402-2416.

Mihanović, H., et al. (2013), Exceptional dense water formation on the Adriatic shelf in the winter of 2012, Ocean Sci. 9, 561–572.

Muench, R. D., A. K. Wåhlin, T. M. Özgökmen, R. Hallberg, and L. Padman (2009), Impacts of bottom corrugations on a dense Antarctic outflow: NW Ross Sea, Geophysical Research Letters, 36, L23607, doi:10.1029/2009GL041347.

Querin, S., G. Cossarini, and C. Solidoro (2013), Simulating the formation and fate of dense water in a midlatitude marginal sea during normal and warm winter conditions, J. Geophys. Res., 118, 885–900, doi:10.1002/jgrc.20092.

Raicich, F., V. Malacic, M. Celio, D. Giaiotti, C. Cantoni, R. R. Colucci, B. Cermelj, and A. Pucillo (2013), Extreme air-sea interactions in the Gulf of Trieste (North Adriatic) during the strong Bora event in winter 2012, J. Geophys. Res. Oceans, 118, 5238–5250, doi:10.1002/jgrc.20398

Rubino, A., D. Romanenkov, D. Zanchettin, V. Cardin, D. Hainbucher, M. Bensi, A. Boldrin, L. Langone, S. Miserocchi, and M. Turchetto (2012), On the descent of dense water on a complex canyon system in the southern Adriatic basin, Continent. Shelf Res., 44, 20-29.

Shapiro, G. I., J. M. Huthnance, and V. V. Ivanov (2003), Dense water cascading off the continental shelf, J. Geophys. Res., 108(C12), 3390, doi:10.1029/2002JC001610.

Smith, P. C., 1976. Baroclinic instabilities in the Denmark Strait overflow. Journal of Physical Oceanography, 6, 355-371.

Smith, R.B. 1979. The influence of mountains on the atmosphere. Advances in Geophysics 21:187-230.

Taviani, M., L. Angeletti, L. Beuck, E. Campiani, S. Canese, F. Foglini, A. Freiwald, P. Montagna, F. Trincardi. On and off the beaten track: megafaunal sessile life and Adriatic cascading processes. This issue.

Tesi T., Langone, L., Goñi, M.A., Turchetto, M., Miserocchi, S., Boldrin, A., 2008. Source and composition of organic matter in the Bari canyon (Italy): dense water cascading vs particulate export from the upper ocean. Deep Sea Res. Part I, 155, 813-831.

Trincardi, F., F. Foglini, G. Verdicchio, A. Asioli, A. Correggiari, D. Minisini, A. Piva, A. Remia, D. Ridente, and M. Taviani (2007), The impact of cascading currents on the Bari Canyon System, SW-Adriatic Margin (Central Mediterranean), Mar. Geol., 246, 208–230.

Turchetto M., Boldrin , A., Langone, L., Miserocchi, S., Tesi, T., Foglini, F., 2007. Particle Transport in the Bari Canyon. Marine Geology, 246, 231-247.

Vilibić, I., N. Supić (2005), Dense water generation on a shelf: the case of the Adriatic Sea, Ocean Dyn., 55, 403–415, doi:10.1007/s10236-005-0030-5.

Vilibić, I., Orlić, M., 2002. Adriatic water masses, their rates of formation and transport through the Otranto Strait. Deep Sea Research I, 49, 1321-1340.

Vilibić, I., Mihanovic´, H., 2013. Observing the bottom density current over a shelf using an Argo profiling float. Geophysical Research Letters, 40, 1-6.

Wåhlin, A., 2004: Topographic advection of dense bottom water, Journal of Fluid Mechanics, 210, 95 - 104.

Wåhlin, A., 2002: Topographic steering of dense bottom currents with application to submarine canyons, Deep-Sea Research part I, 49 (2), 305 - 320.

Wåhlin, A. and G. Walin, 2001: Downward migration of dense bottom currents. Environmental Fluid Mechanics 1 (2), 257 - 279.

Figure captions:

Figure 1: Adriatic Sea bathymetry (colour, m). The red box indicates the location of the Bari Canyon System and the green circle is the Gondola Slide. In the upper right panel is the Mediterranean Sea with the square indicating the Adriatic Sea.

Figure 2: Locations of CTD, XBT (leg 1, left panel, leg 2, middle panel) and moorings (right panel). Isobaths (coloured lines) are draw every 50 m.

Figure 3: Θ-S plot: in orange leg 1a, in grey leg 1b, in red leg 2

Figure 4: Mean bottom (0 mab -10 mab) in-situ temperature with baroclinc currents (arrows), potential density anomaly and DO, leg 1a (23-25 March). Transect A is the northernmost crossshore transect, transect B is the southernmost crossshore transect.

Figure 5: Averaged bottom (0 mab -10 mab) in-situ temperature with baroclinc currents (arrows), potential density anomaly and DO, leg 1b (29 March – 1 April).

Figure 6: Averaged bottom (0 mab -10 mab) in-situ temperature with baroclinc currents (arrows), salinity and DO, leg 2 (14-20 April).

Figure 7: Temperature (left), Salinity (middle) and DO (right) from CTDs collected during Leg1 (23 Marc – 1 Apr; upper panels) and Leg 2 (14 -20 April; lower panels).

Figure 8 Temperature from transect A (upper panel) and transect B (lower panel), carried out respectively on 25 March and 24 March. Grey lines indicate CTD casts, black lines XBT casts.

Figure 9: CTD casts at stations 039b and 043, showing potential density anomaly (blue), potential temperature (green), salinity (red) and DO (cyan). To the left, vertical profile of LADCP currents.

Figure 10: CTD casts at stations 029 and 030, showing potential density anomaly (blue), potential temperature (green), salinity (red) and DO (cyan). To the left, vertical profile of LADCP currents.

Figure 11: Time series of potential temperature (left panels) and currents (right panels) at 8 mab from moorings.

Figure 12: Rose plots of currents (cm/s) with potential temperature (colour map, °C) of mooring data at 8 mab.

Figure 13: Zoom on cascading area upstream FF during Leg 2 (14-20 April). Circles are proportional to the benthic layer height based on the $\theta < 12.9$ °C threshold (stars means missing BL according to the threshold chosen), arrows are currents averaged over the benthic layerL (black) or bottom currents (red). Colour map is potential temperature averaged over the benthic layer (°C).

Figure 14: Time series of magnitude of the currents and potential temperature from mooring FF. Grey boxes indicate timing of the surveys by the R/V.

Figure 15: CTD casts at stations 014 and 017 carried out on 24 March, showing potential density anomaly (blue), potential temperature (green), salinity (red) and DO (cyan). To the left, vertical profile of LADCP currents.

Figure 16: Median currents magnitude (upper panel), and median direction (lower panel) from downward-looking ADCP data at, from 100 mab to the bottom, during cascading events only, observed at moorings BB, CC, FF. Dots in the upper panel are median currents from current meters at 8 mab.

Tables Captions:

Table 1: Dynamics parameters evaluation on transect A (based on CTD 39b and 43b, local maxima of NAdDW) and transect B (based on CTD 29 and 30, local maxima of NAdDW). The slope is estimated using adjacent CTDs. δ estimated as Cd*g'*slope/f^2 using Cd=1.3e-3. g' and R are computed assuming 1.5 reduce gravity model.

Table 1

	CDT39b	CTD43b	CDT 29	CTD 30
g'	2.5e-3 m/s2	2.8e-3 m/s2	3.0e-3 m/s2	2.3e-3 m/s2
α	2.3e-3	2.4e-3	5.7e-3	1.19e-2
f	9.8e-5 s-1	9.76e-5 s-1	9.75e-5 s-1	9.75e-5 s-1
W	50 km		40 km	
H	35	20 m	30 m	15 m
R	3 km	2.4 km	3.1 km	2 Km
δ	1 m	1 m	2.4 m	3.7 m

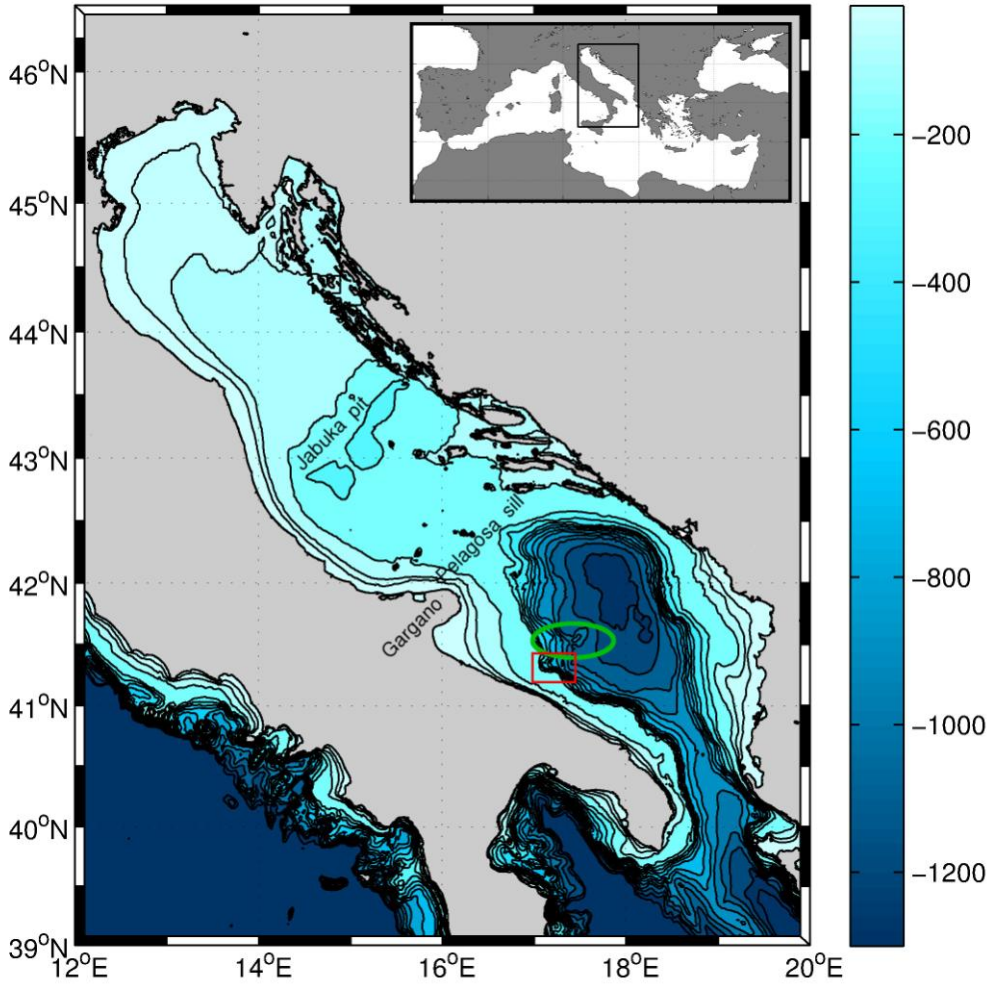

Figure 1

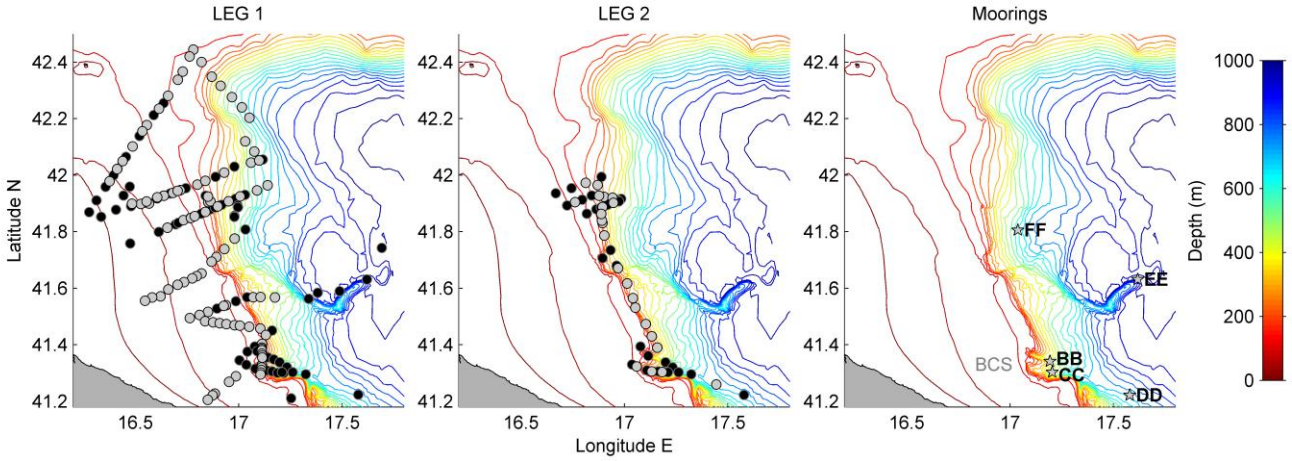

Figure 2

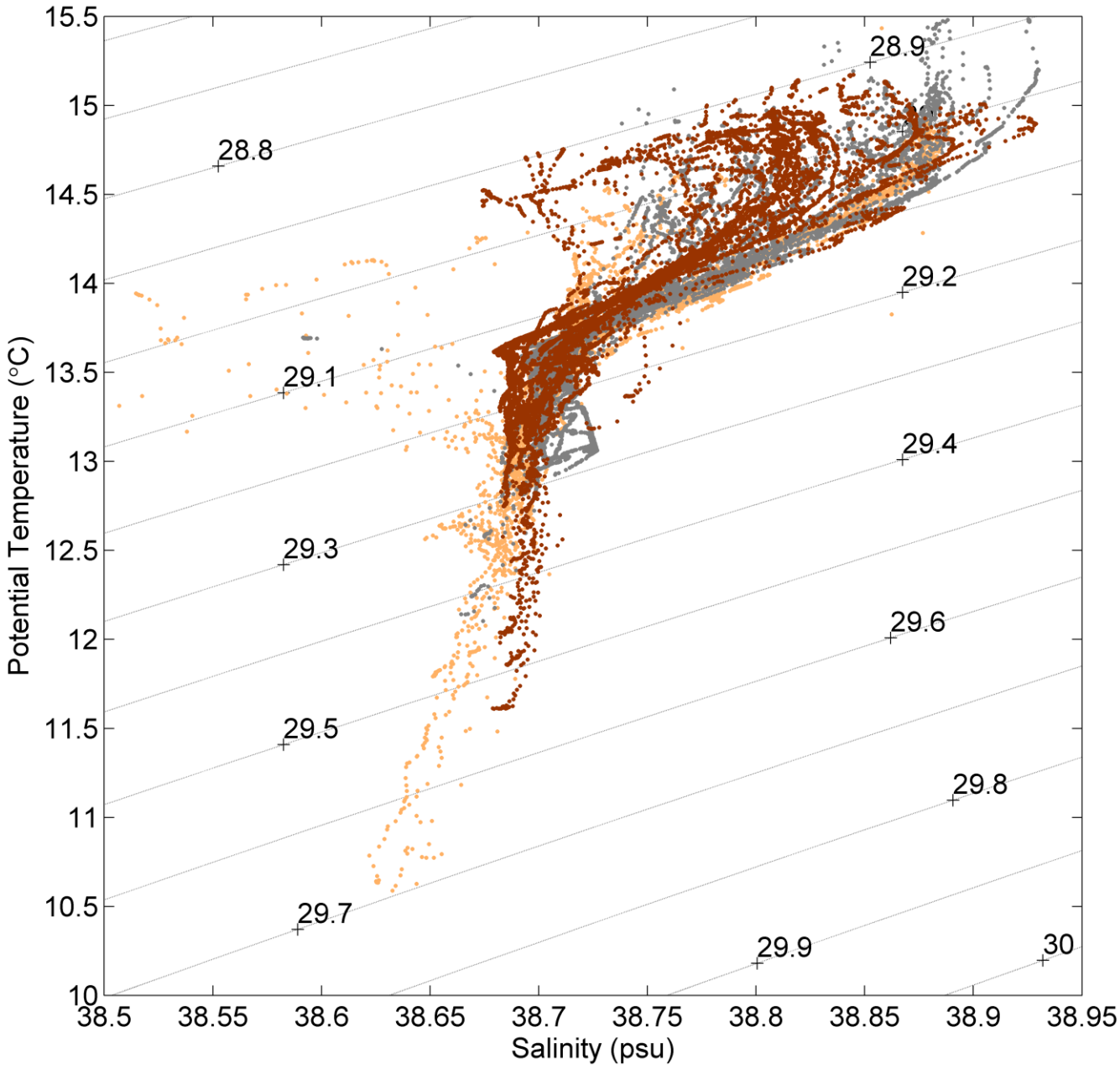

Figure 3

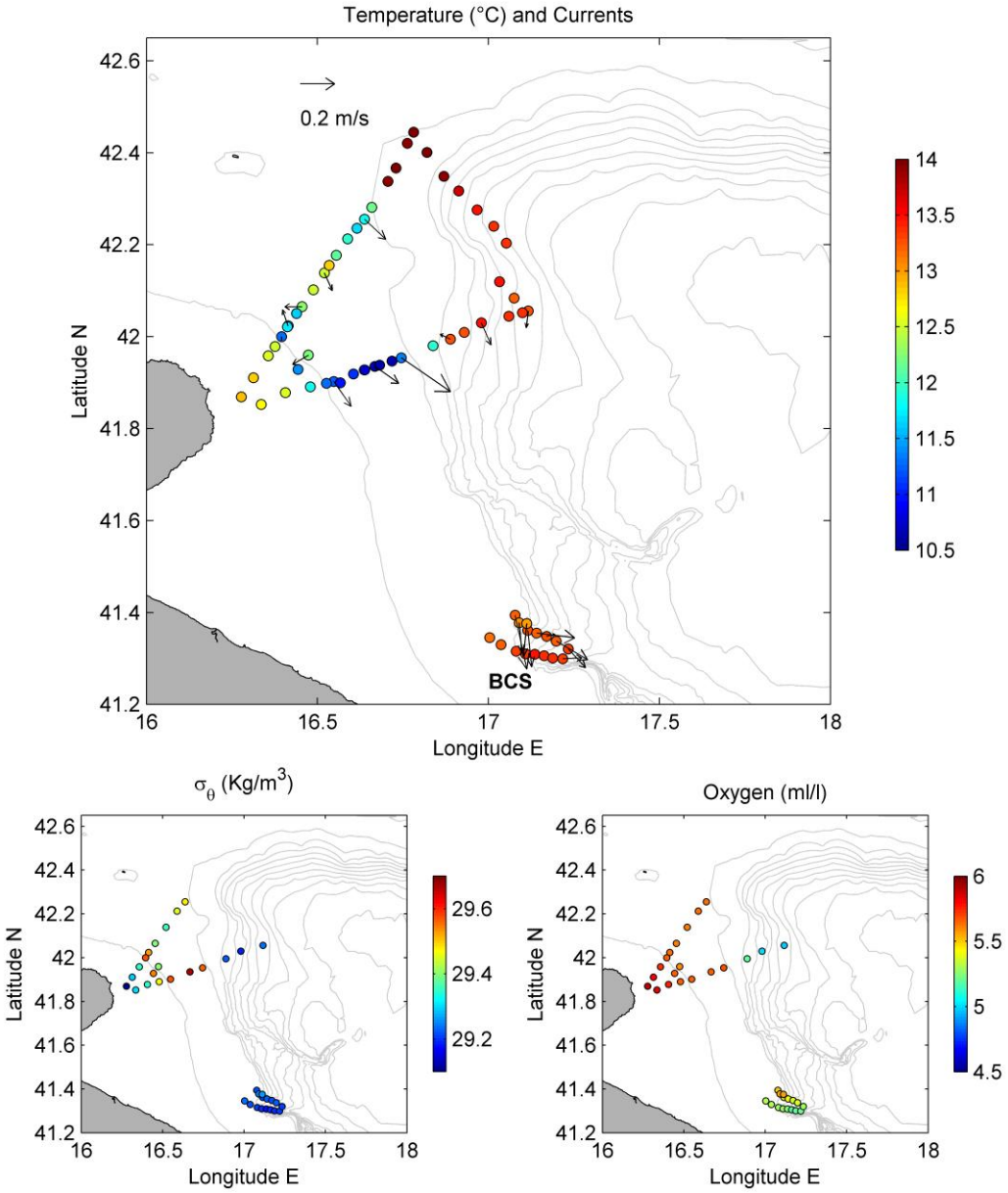

Figure 4

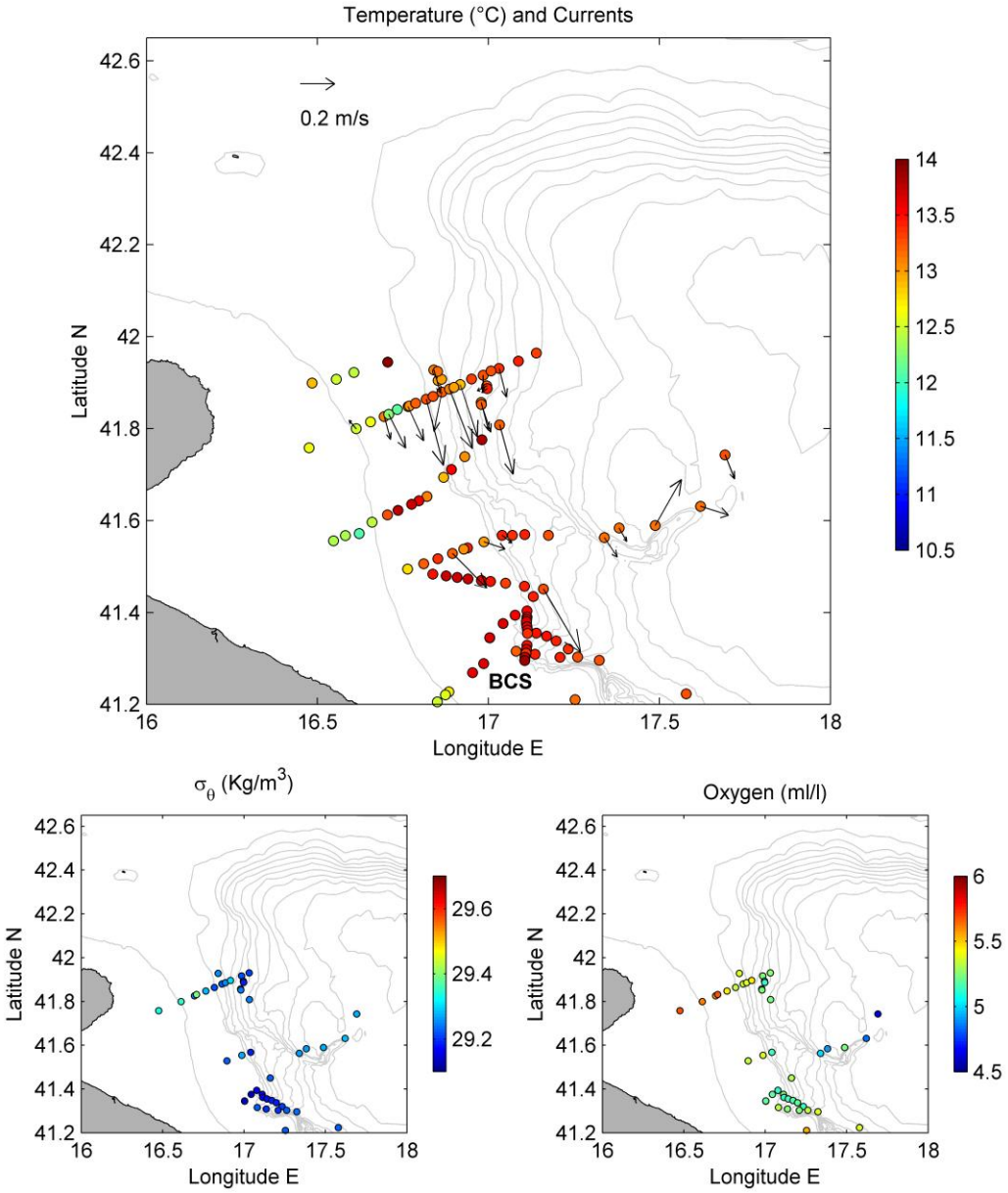

Figure 5

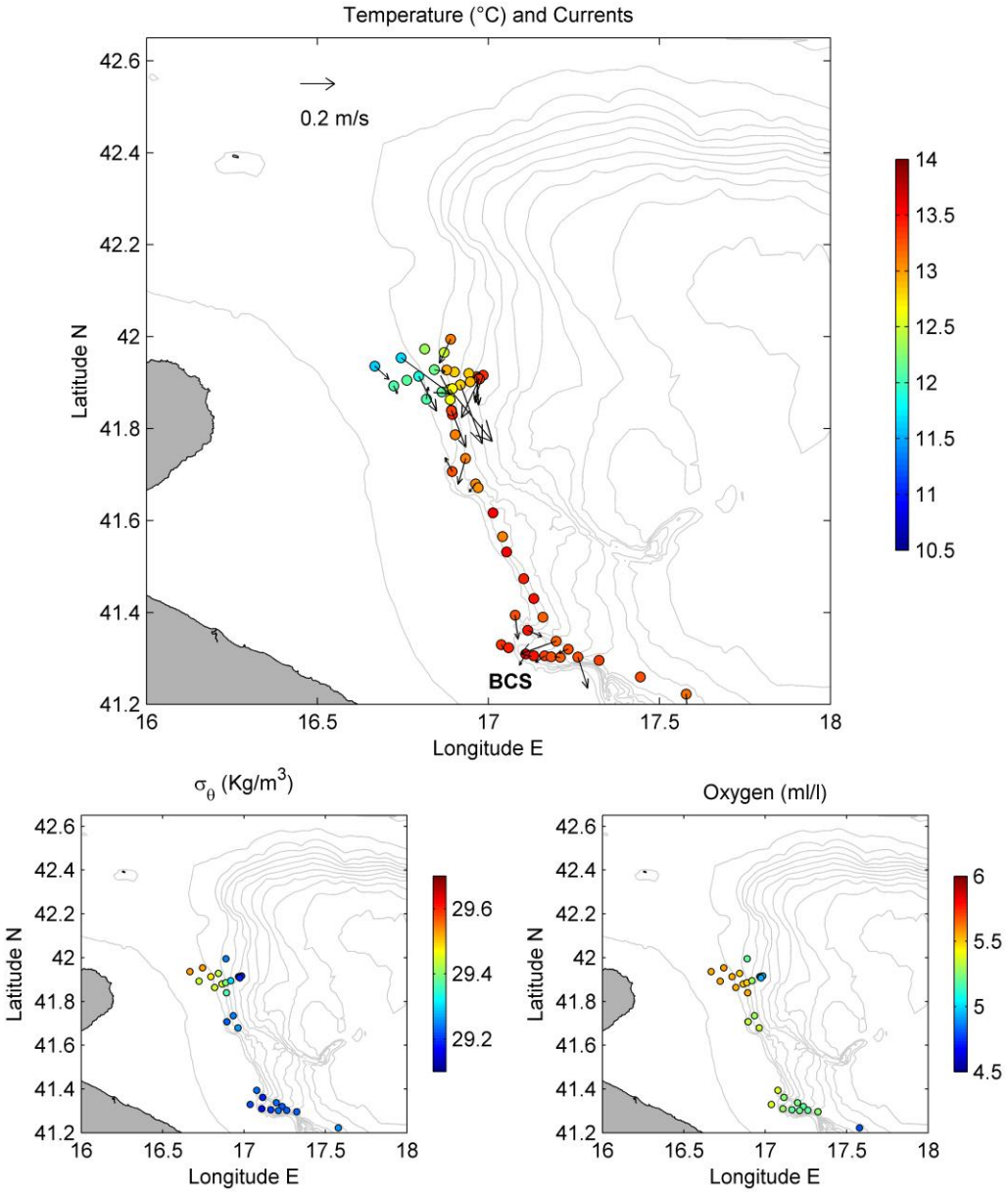

Figure 6

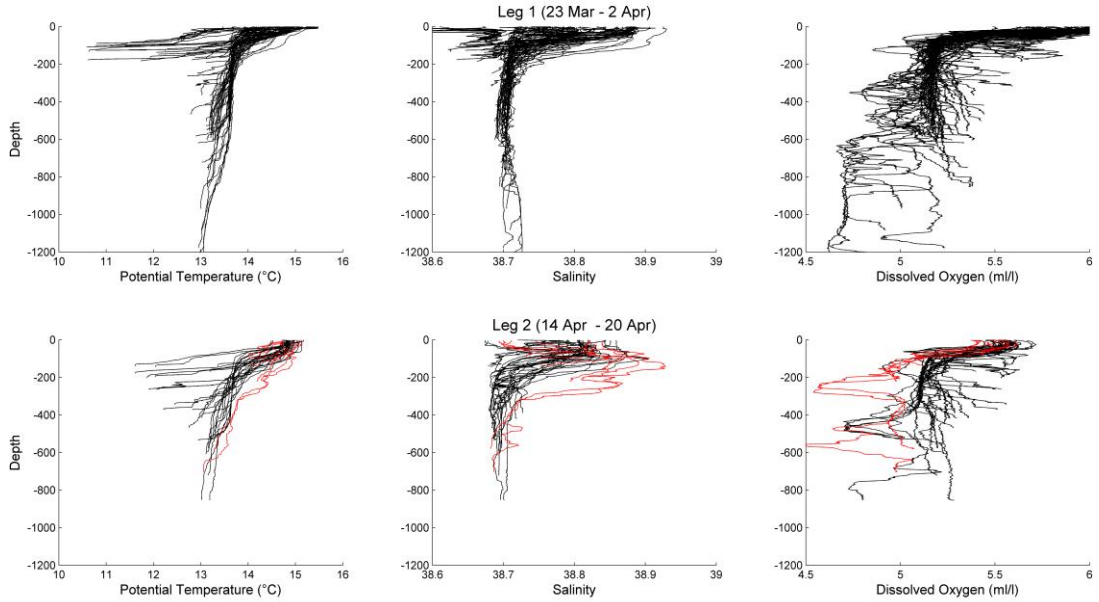

Figure 7

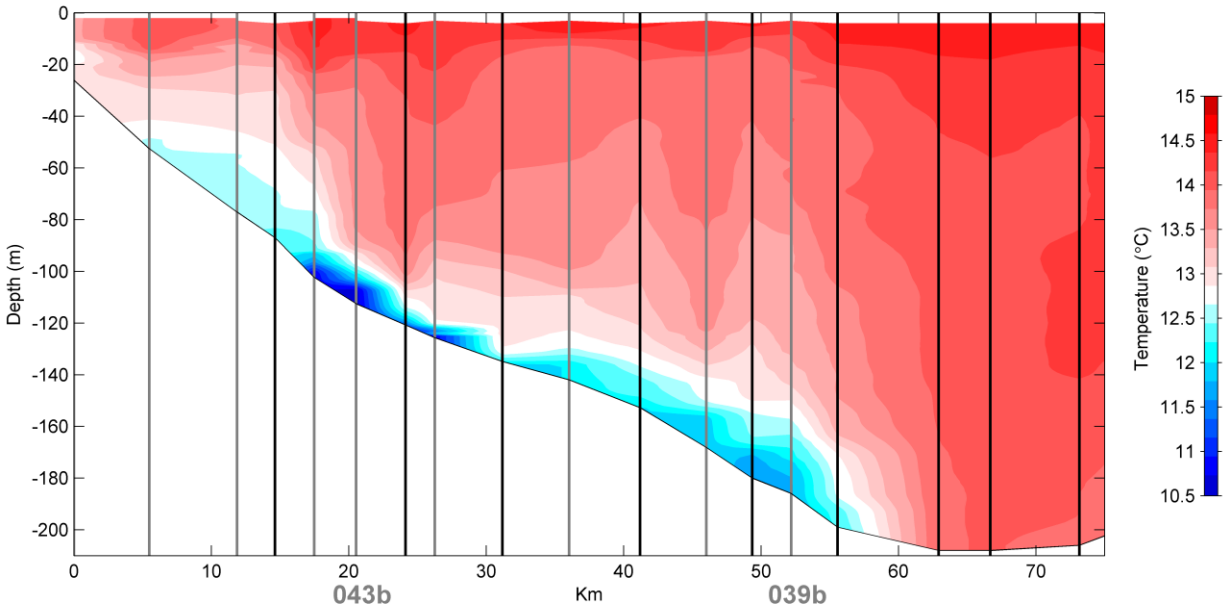

Figure 8a

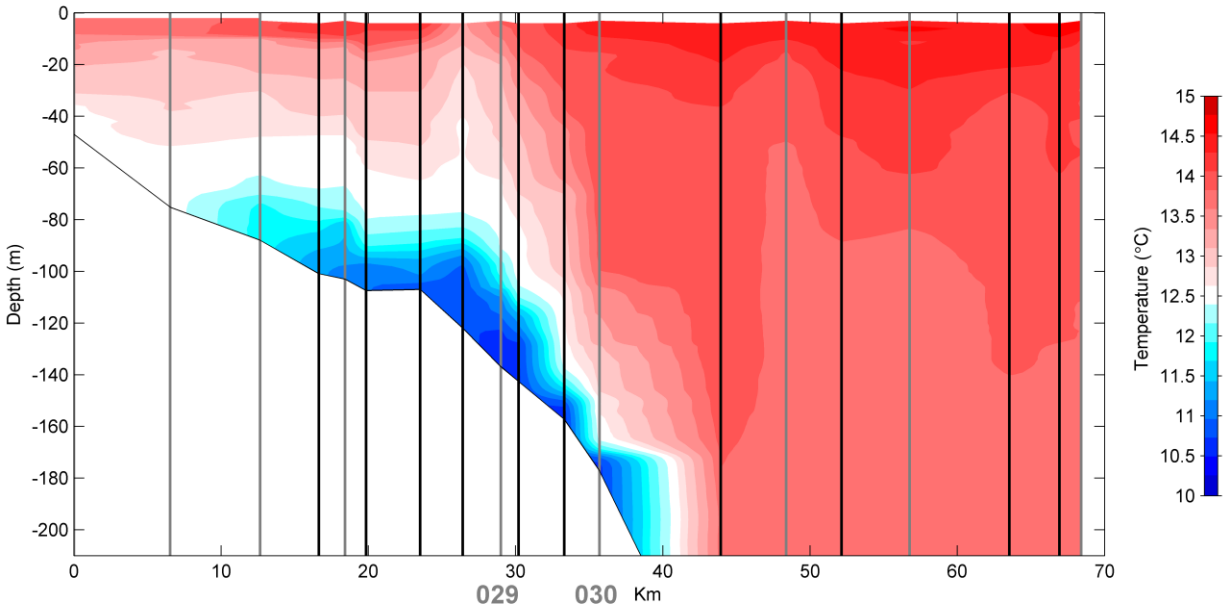

Figure 8b

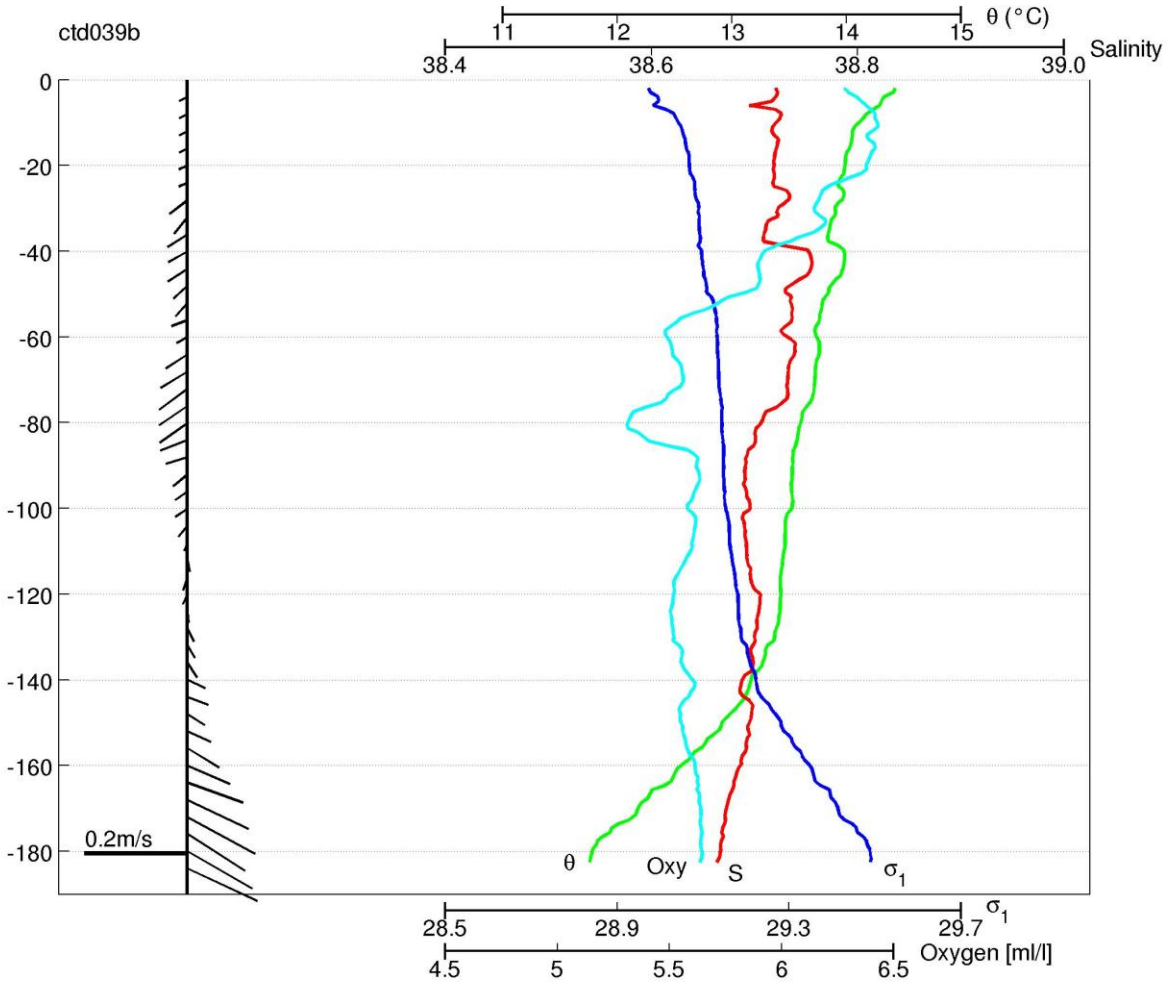

Figure 9a

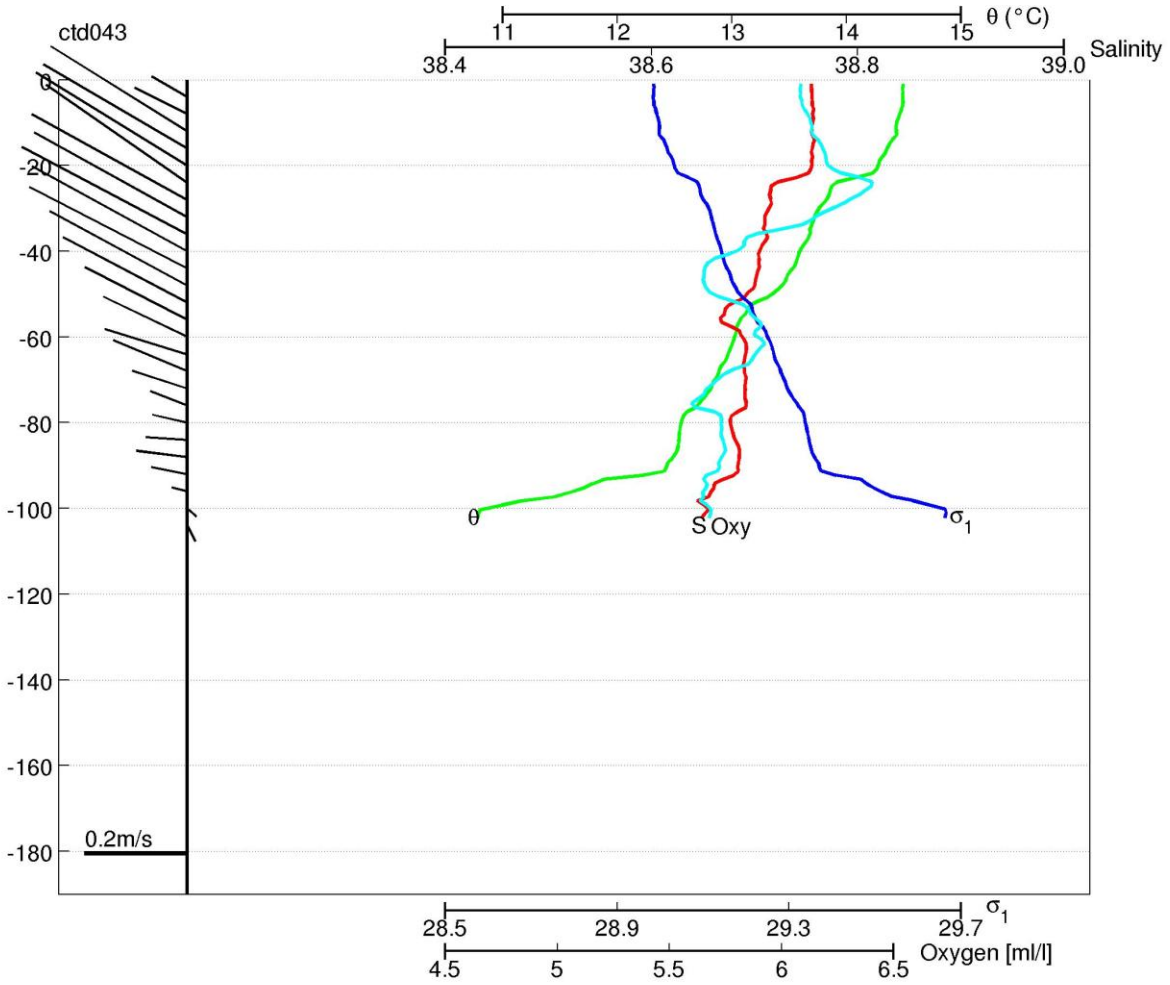

Figure 9b

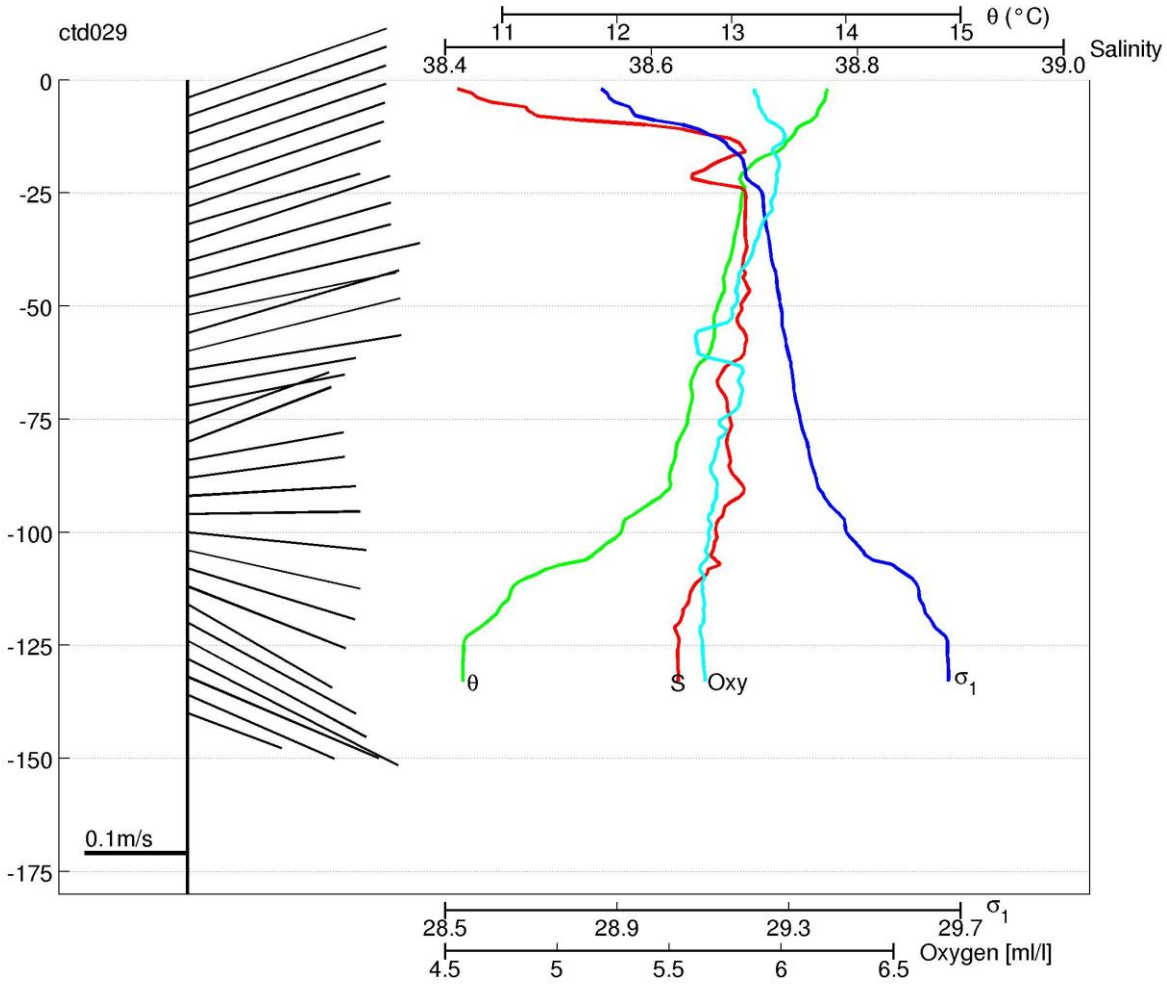

Figure 10a

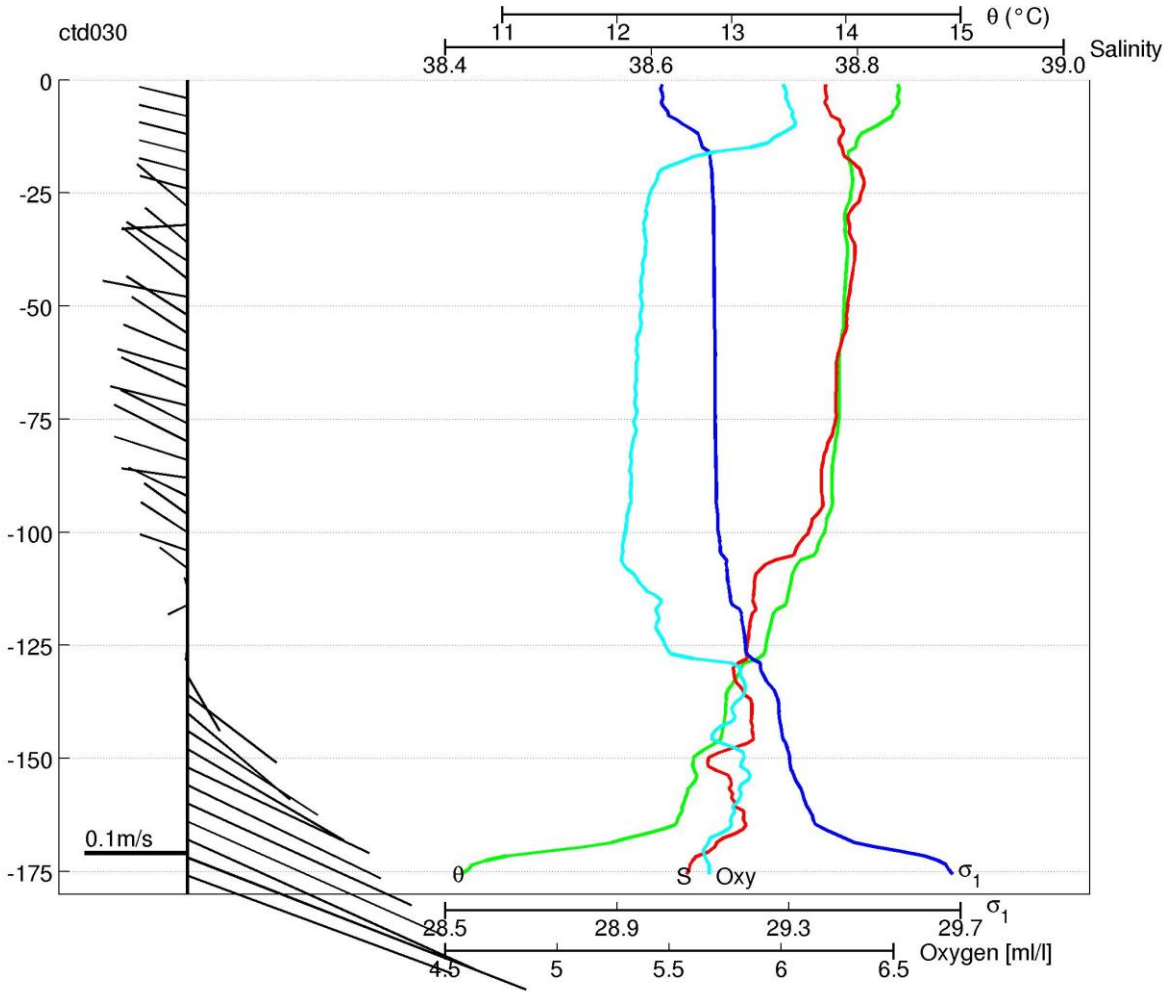

Figure 10b

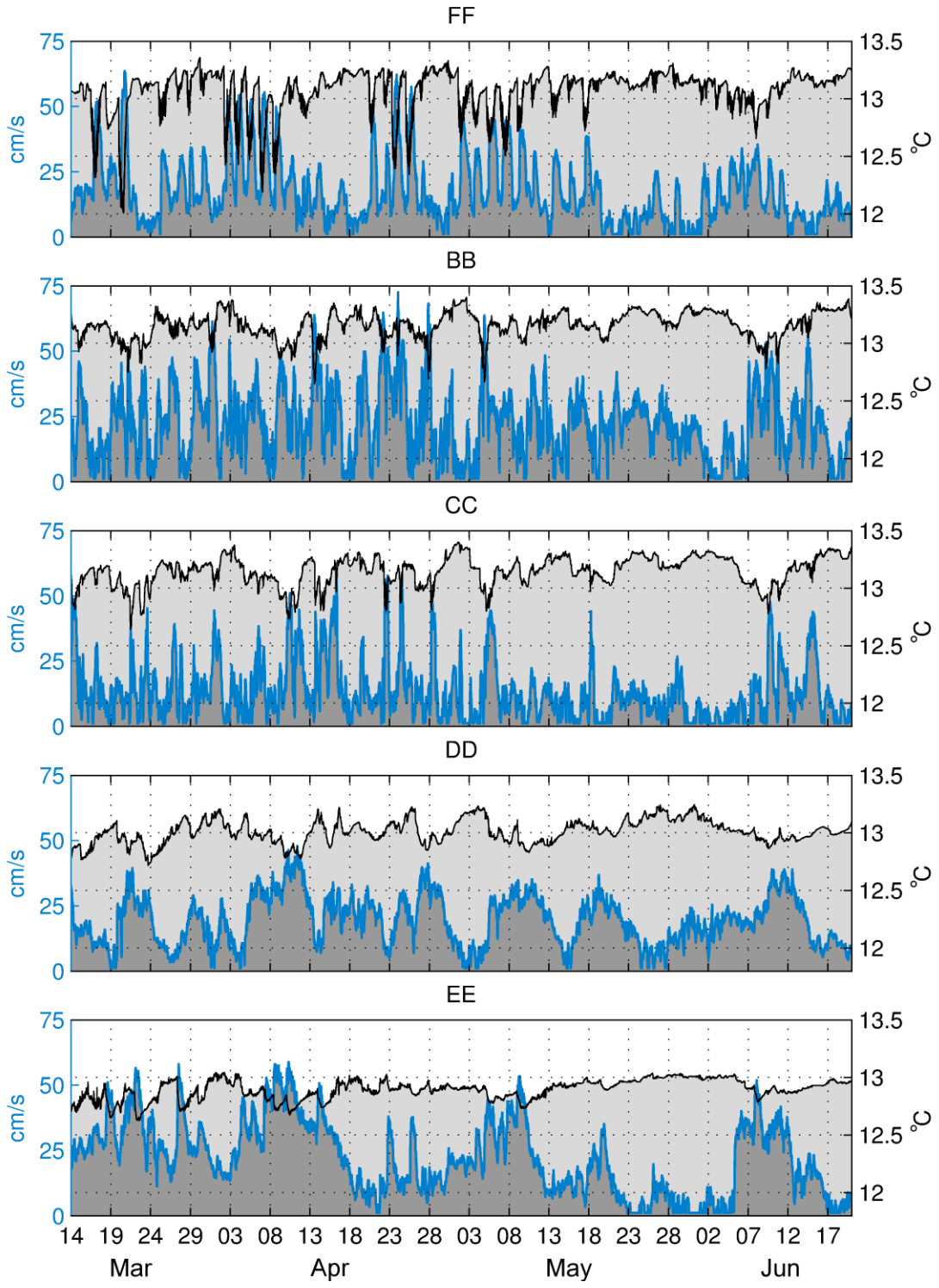

Figure 11

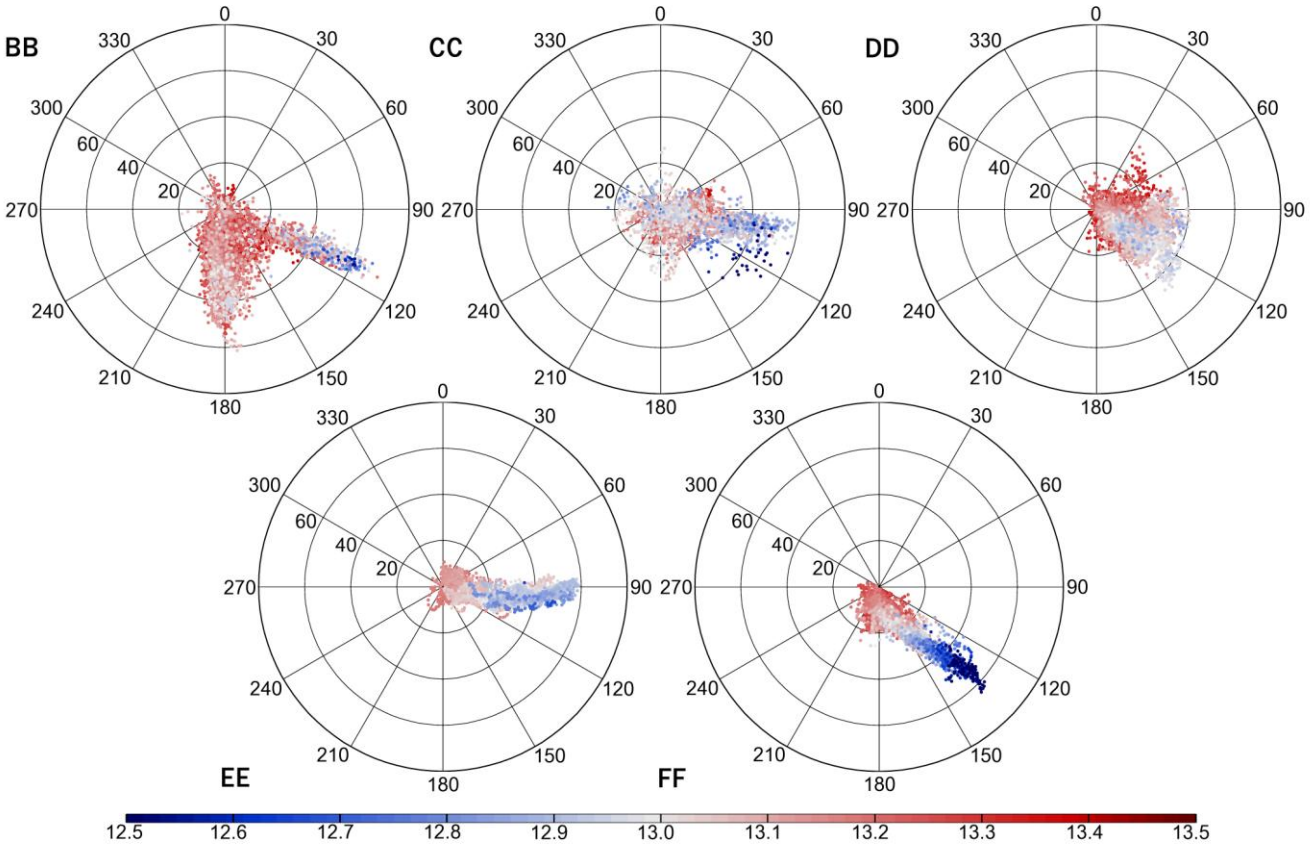

Figure 12

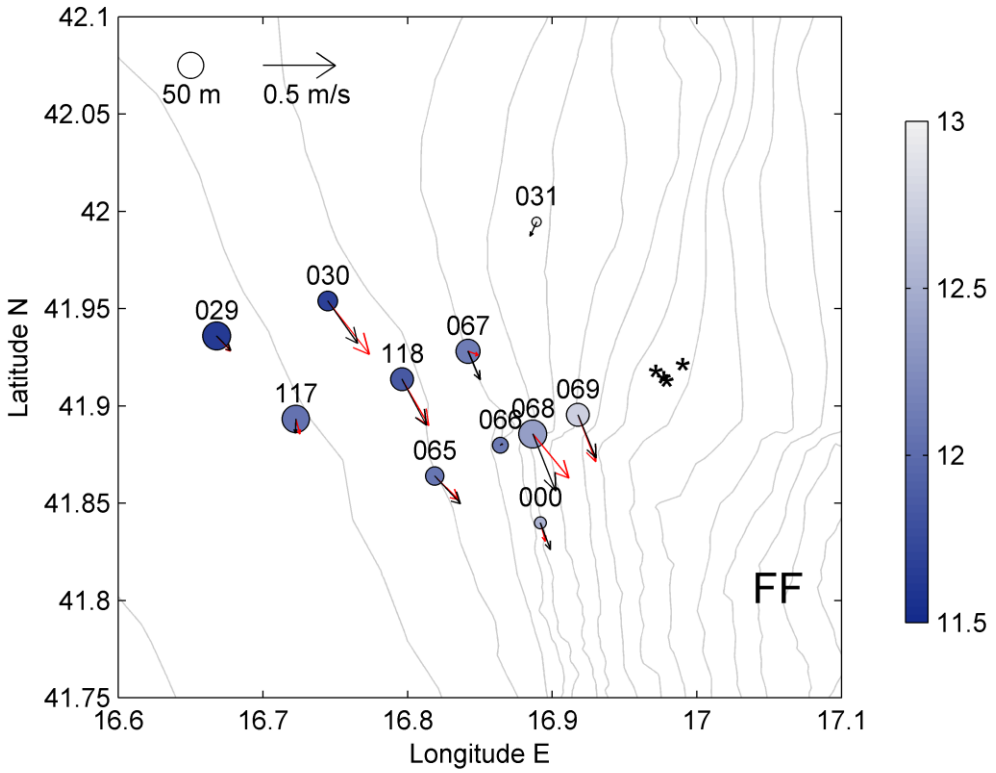

Figure 13

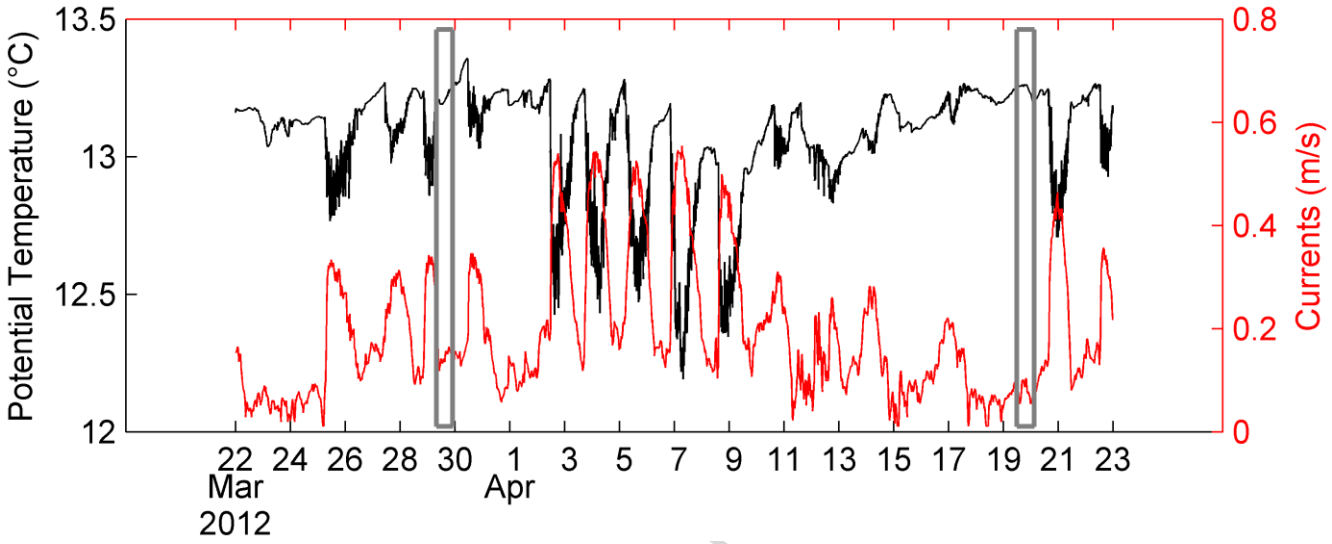

Figure 14

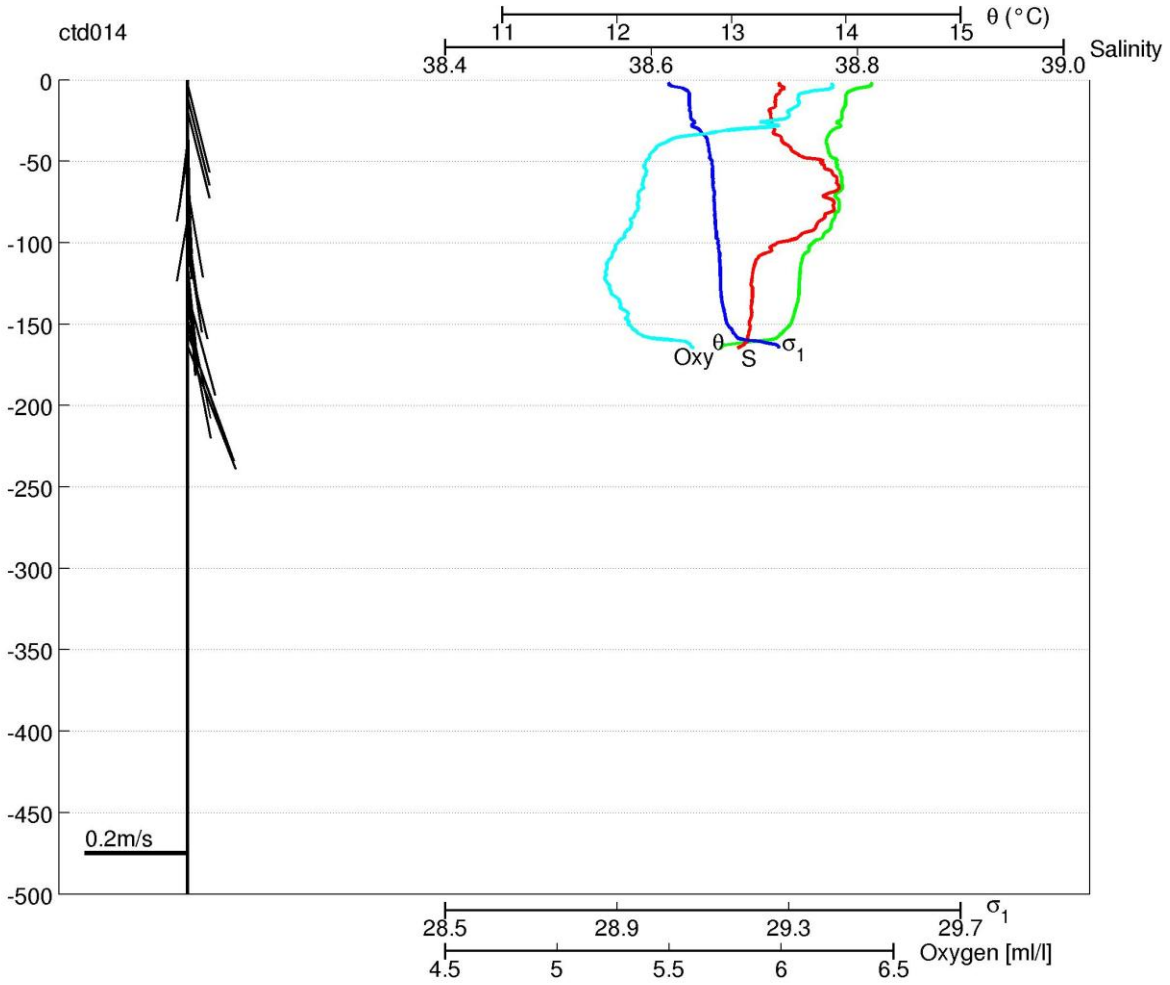

Figure 15a

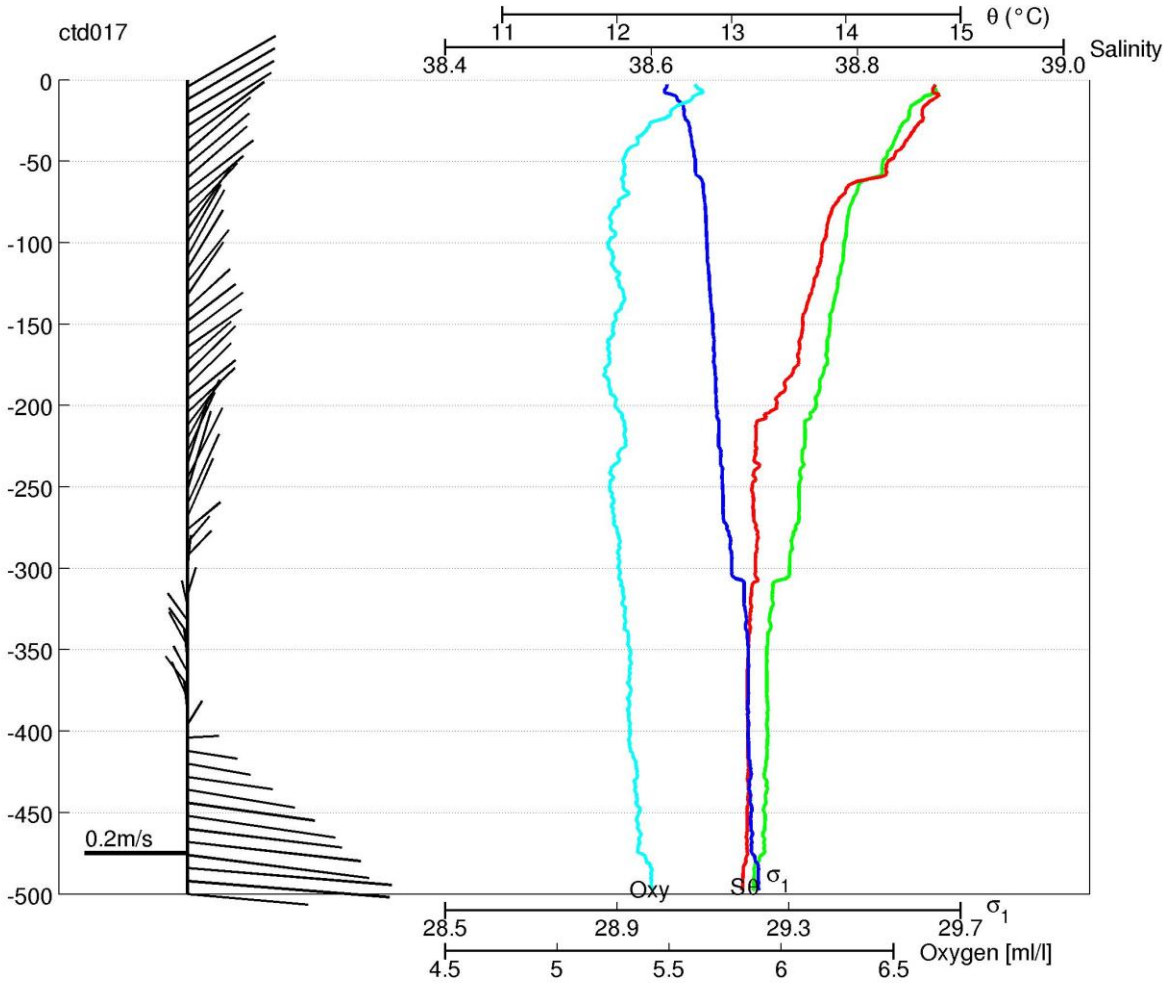

Figure 15b

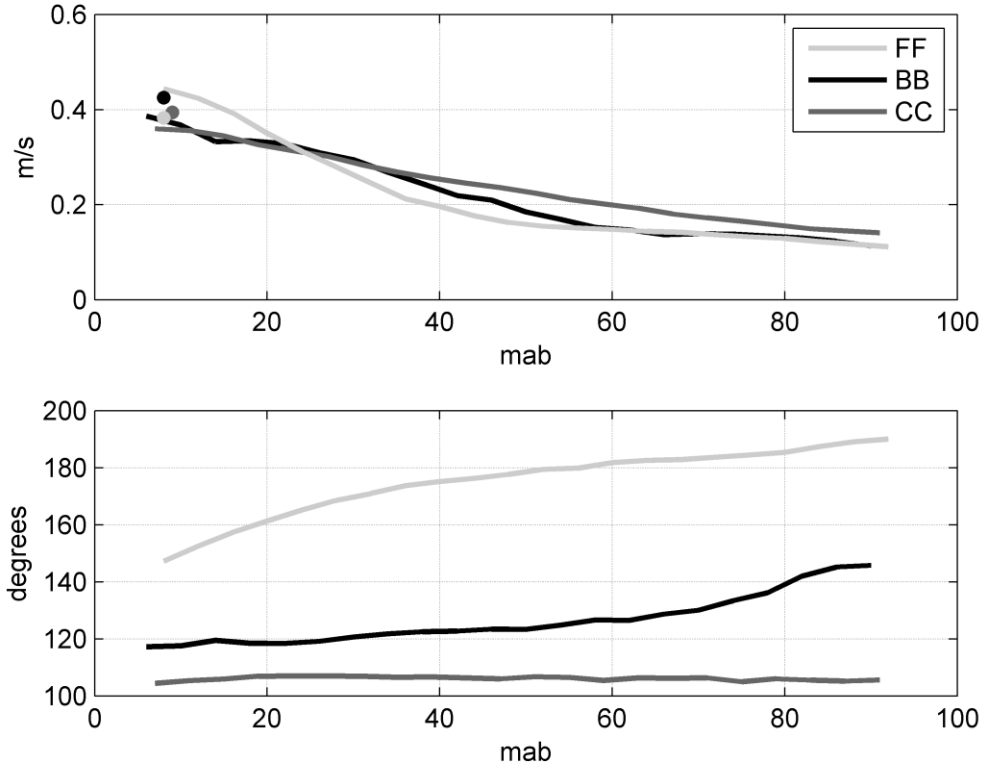

Figure 16